



Research article

Photo-sono activated BNT@MoS₂ composites for rapid eradication of breast cancer

Rong Li^{a,b,1}, Hao Liu^{a,c,1}, Xiudong Guo^a, Xin yang^a, Hailiang Zhang^a, Jianbo Song^{a,b,**}, Guannan Zhang^{a,b,*}

^a Third Hospital of Shanxi Medical University, Shanxi Bethune Hospital, Shanxi Academy of Medical Sciences, Tongji Shanxi Hospital, Taiyuan, 030032, China

^b Shanxi Provincial Key Laboratory for Translational Nuclear Medicine and Precision Protection, Taiyuan, 030006, China

^c Shanxi Medical University, Taiyuan, 030001, Shanxi Province, China

ARTICLE INFO

Keywords:

Biomaterials
Composite materials
Piezoelectric
Photothermal therapy
Sono-dynamic therapy
Breast cancer

ABSTRACT

Non-invasive external energy triggered efficient tumor therapy is a promising specific treatment strategy. Herein, a composite material of bismuth sodium titanate (BNT) and molybdenum disulfide (MoS₂) with piezoelectric effect was designed for the synergistic treatment of breast cancer with near-infrared-II (NIR-II) light and ultrasound (US) activation. The BNT@MoS₂ exhibit excellent photothermal and acoustic properties upon excitation by 1060 nm NIR-II laser and US, respectively. The synergistic effect of hyperthermia and reactive oxygen species (ROS) under photoacoustic action endows the BNT@MoS₂ with remarkable anti-tumor activities, enabling them to eradicate breast cancer cells within 10 min. The work could provide new insights into the treatment of breast cancer.

1. Introduction

To date, cancer remains a prominent and formidable threat to humanity. Conventional cancer treatment modalities encompass surgical intervention, radiation therapy, and chemotherapy, which often entail invasiveness and give rise to undesirable side effects [1]. Hence, the development of innovative cancer therapeutic approaches with reduced invasiveness and lower side effects is of utmost importance. Non-invasive external energy-triggered efficient oncotherapy, due to its high tumor specificity, excellent controllability, therapeutic efficacy, and mitigated damage to normal organs/tissues, is regarded as one of the most promising therapeutic strategies [2]. Ultrasound (US) is one of the most explored physical triggers owing to its non-invasiveness, deep tissue penetration, and cost-effectiveness. Particularly, US-triggered sono-dynamic therapy (SDT) has demonstrated effectiveness in generating cytotoxic reactive oxygen species (ROS) by employing carefully designed sonosensitizers [3]. In addition, light, especially near-infrared (NIR) light, has found extensive applications in phototherapy encompassing photothermal therapy (PTT) and photodynamic therapy (PDT). The NIR-II biowindow (1000–1350 nm), owing to its superior tissue penetration capability and higher maximum permissible exposure

* Corresponding author. Third Hospital of Shanxi Medical University, Shanxi Bethune Hospital, Shanxi Academy of Medical Sciences, Tongji Shanxi Hospital, Taiyuan, 030032, China.

** Corresponding author. Third Hospital of Shanxi Medical University, Shanxi Bethune Hospital, Shanxi Academy of Medical Sciences, Tongji Shanxi Hospital, Taiyuan, 030032, China.

E-mail addresses: jianbo2611@sxmu.edu.cn (J. Song), 815760979@qq.com (G. Zhang).

¹ The first two authors contributed equally to this work.

<https://doi.org/10.1016/j.heliyon.2024.e25023>

Received 6 December 2023; Received in revised form 28 December 2023; Accepted 18 January 2024

Available online 21 January 2024

2405-8440/© 2024 The Authors. Published by Elsevier Ltd. This is an open access article under the CC BY-NC-ND license (<http://creativecommons.org/licenses/by-nc-nd/4.0/>).

limit (MPR), exhibits a more favorable therapeutic efficacy compared to the conventional NIR-I biowindow (750–1000 nm) [4].

Recently, inorganic piezoelectric nanomaterials with piezoelectric effects, such as BaTiO₃, ZnO, and Bi₂MoO₆, have emerged as hotspot sensitizers for cancer SDT, as they efficiently generate ROS through piezo-catalysis under ultrasonic irradiation [5]. Upon exposure to mechanical vibrations, such as US, piezoelectric materials can be polarized, resulting in dynamically evolving internal electric fields [6]. These electric fields drive the migration of ultrasound-induced electrons (e⁻) and holes (h⁺) towards opposing surfaces, subsequently engaging in redox reactions with neighboring oxygen-containing molecules, leading to the generation of singlet oxygen (¹O²), superoxide anion (•O²⁻), or hydroxyl radicals (•OH) [7]. However, in piezoelectric sensitizers, the rapid recombination of US-generated e⁻ and h⁺ often limits the production of ROS.

Recently, researchers have employed various strategies to address this limitation, including material composites, the construction of heterojunctions, and the introduction of defects [8]. Material composites have been implemented to promote charge separation and inhibit electron-hole recombination, thereby enhancing ROS generation. The Bismuth Sodium Titanate (BNT) is a piezoelectric ceramic material that exhibits exceptional piezoelectric properties and thermal stability, while also demonstrating distinctive catalytic characteristics, rendering it extensively employed in the domains of catalysis and medicine [9]. Molybdenum disulfide (MoS₂) belongs to the family of layered transition metal disulfide compounds, and has garnered increasing attention in PTT due to its excellent biocompatibility, large surface area, and high photothermal conversion efficiency within the NIR. In addition, it can improve the catalytic efficiency when combined with some materials [10–12].

Herein, we have successfully synthesized BNT and MoS₂ composites for SDT and PTT combined treatment of breast cancer. The BNT@MoS₂ composite was synthesized through a simple two-part hydrothermal method, exhibiting excellent photothermal properties under NIR-II irradiation. Moreover, its piezoelectric effect can promote the migration of e⁻ and h⁺ generated by US, thereby improving the efficiency of SDT. This piezoelectric composite provides a promising approach to treating breast cancer.

2. Materials and methods

2.1. Sample preparation and characterization

The BNT was synthesized using the hydrothermal method, employing Bi(NO₃)₃·5H₂O, Bi(OH)₃, Ti(OC₄H₉)₄, and NaOH as hydrothermal solvents. The bismuth concentration was maintained at 0.1 M with a stoichiometric ratio of Bi/Ti set to 0.5. A NaOH concentration of 12 M and a hydrothermal time of 24 h were employed to obtain the desired BNT material. The BNT surface was coated with MoS₂ using a secondary hydrothermal method. Thioacetamide (50 mg) and sodium molybdate (25 mg) were added to 50 mL of deionized water and completely dissolved. Subsequently, BNT was introduced into a hydrothermal reactor and heated at 200 °C for 24 h, resulting in the formation of BNT@MoS₂.

The morphology of the materials was observed using Field Emission Scanning Electron Microscopy (FE-SEM, JSM-7001F, JEOL) and High-Resolution Transmission Electron Microscopy (HR-TEM, JSM-2010, JEOL). The phase composition and surface chemical composition were analyzed using HR-TEM, X-ray Diffraction (XRD, Rigaku Dmax-3C), and X-ray Photoelectron Spectroscopy (XPS, Thermo). The piezoelectric properties of the materials were measured by piezoelectric response force microscopy (PFM, Bruker Dimension Icon). The scanning frequency and scanning area are 0.5 Hz and 2 μm, respectively. The ESR spectrometer (EMXPLUS10/12, Bruker, Germany) was used to test ESR, and the ultrasonic parameters used in the experiment were 1.0 MHz, 1.5 W/cm², 50 % duty cycle [13,14].

2.2. Photothermal effect in Vitro

The sample (1 mL, 1 mg/mL) was placed into a 24-well plate and exposed to a 1060 nm laser (0.8 W/cm²) for a duration of 10 min. Real-time temperature measurements were conducted every 1 min using an infrared thermal imager. In addition, the temperature changes of different laser power (0.6–1.0 W/cm²) and different sample concentration (0.5–1.5 mg/mL) were recorded respectively.

2.3. Evaluation of antitumor ability in vitro

4T1 murine breast cancer cells were obtained Shanghai Chinese Academy of Sciences. The cells were cultured in a high-sugar DMEM medium supplemented with 10 % (v/v) fetal bovine serum and 1 % (v/v) penicillin/streptomycin. After 1 mL cells (1 × 10⁴ cells/cm²) were cultured for one day, the samples (1 mg/mL) were employed to evaluate the cytotoxicity against tumor cells following various treatments (Light, US, Light + US, 10 min). The killing effect of tumor cells was evaluated by live/dead staining and MTT methods (The specific method was in the supplementary information).

The elimination of breast cancer cells was evaluated by live/dead staining. The cells were cultured for one day and subsequently washed with PBS. Afterwards, 100 μL of stain was added to the 24-well plate and incubated in darkness for a duration of 40 min. Subsequently, four fields were randomly selected to be photographed under a confocal scanning laser microscope (CLSM).

The cytotoxicity was assessed using the MTT assay. After different treatments, the cells were immersed in 900 μL of medium and 100 μL of MTT before being incubated for a duration of 4 h. The liquid was subsequently removed and replaced with 1 mL of dimethyl sulfoxide to dissolve any crystals present on the sample surface. Finally, the absorbance level of the solution was measured at a wavelength of 492 nm.

The morphology of cells was analyzed using cytoskeleton assembly. After different treatments, the cells were fixed in 4 % paraformaldehyde for 45 min and subsequently stained with FITC and DAPI for 40 and 10 min, respectively. Multiple regions were

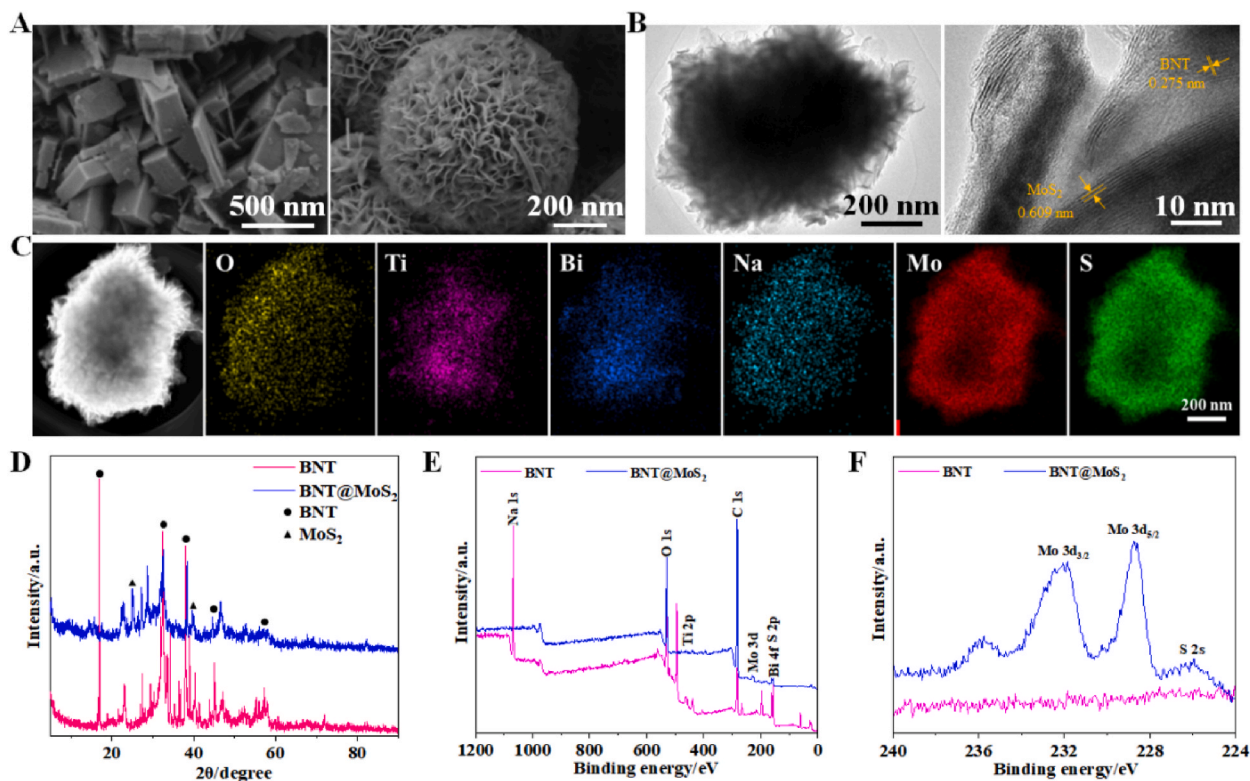


Fig. 1. (A) SEM images of BNT and BNT@MoS₂; (B) TEM images and (C) elemental maps of BNT@MoS₂; (D) XRD patterns; (E) XPS survey spectra of BNT and BNT@MoS₂ and (F) High-resolution XPS spectra of Mo 3d of BNT and BNT@MoS₂.

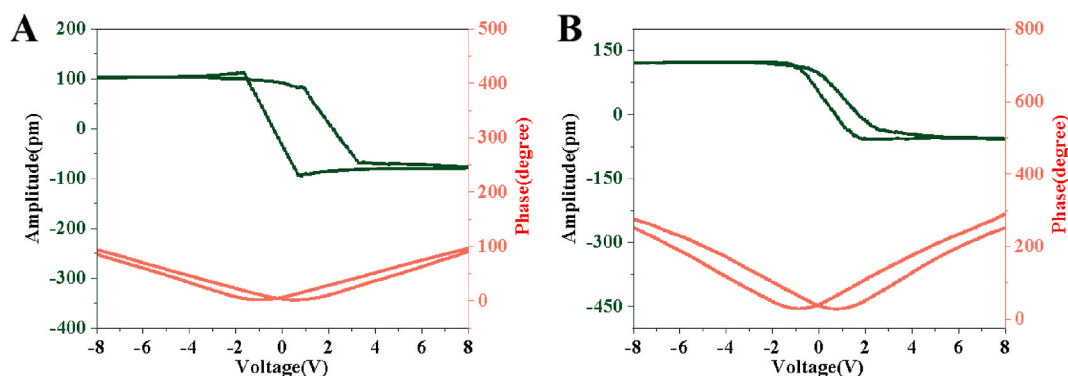


Fig. 2. (A) The PFM results of BNT and (B) BNT@MoS₂.

randomly selected for observation of cellular morphology using CLSM, generating corresponding images.

3. Results and discussion

3.1. Characterization of BNT@MoS₂

The morphologies of BNT and BNT@MoS₂ generated by hydrothermal process were shown in Fig. 1A and B. BNT was a homogeneous cubic particle, and BNT@MoS₂ was a nanowire-like MoS₂ growing around BNT. Over the past 20–30 years, researchers have come to a consensus that nanoparticle size determines its biological distribution, tumor penetration, cell internalization, etc., all of which have a pivotal influence on the overall therapeutic effectiveness of cancer. Most currently approved anti-cancer nanomedicine particles have a size range of 100–200 nm, as smaller nanomaterials have greater tissue penetration and greater tumor inhibition. Therefore, the size of BNT@MoS₂ needs to be further optimized. High-resolution TEM imaging at BNT@MoS₂ observed BNT with

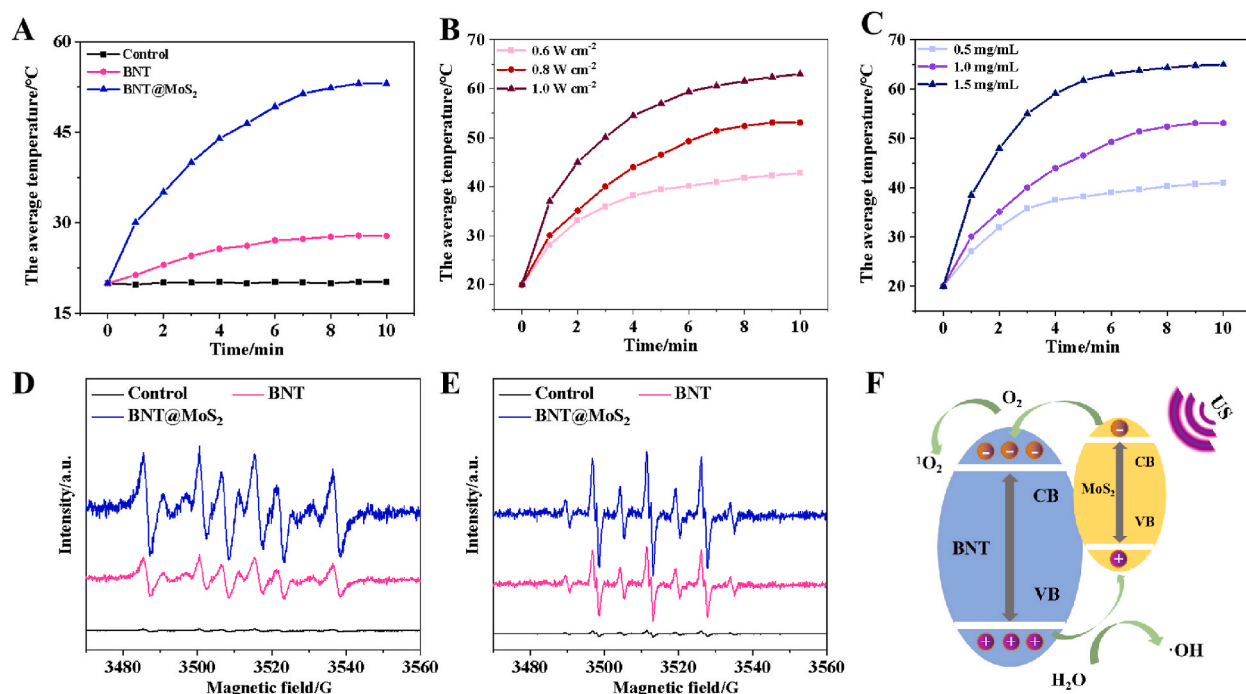


Fig. 3. Photothermal and acoustodynamic properties of samples under 1060 nm laser and US irradiation: (A) photothermal rise curves of BNT and BNT@MoS₂; (B) temperature rise curves of BNT@MoS₂ under different laser power (0.6–1.0 W/cm²); (C) temperature rise curves of different concentrations BNT@MoS₂ (0.5–1.5 mg/mL); (D) ¹O₂ and (E) ·OH detected from samples by ESR with the DMPO probe; (F) schematic of acoustodynamic performance of BNT@MoS₂.

lattice spacing of 0.275 nm and MoS₂ at 0.609 nm, respectively (Fig. 1B). The EDS element map for BNT@MoS₂ showed a uniform distribution of O, Ti, Bi, Na, Mo, and S (Fig. 1C).

Fig. 1D showed the XRD patterns of BNT and BNT@MoS₂. The typical diffraction peaks of BNT were detected in both BNT and BNT@MoS₂, but the peaks of BNT were decreased in BNT@MoS₂. In addition, the diffraction peak of MoS₂ corresponding to plane (110) at 38.413° was found in BNT@MoS₂, indicating that MoS₂ had successfully grown on the surface of BNT.

The surface chemical states of BNT and BNT@MoS₂ were analyzed by XPS (Fig. 1E). The XPS spectra of BNT showed the presence of C, O, Ti, Bi and Na, respectively. BNT@MoS₂ also detected the above elements, but the peaks of Na, Ti and Bi decreased significantly. In addition, the presence of S and Mo was also detected, which also indicated that MoS₂ was fixed on the surface of BNT (Fig. 1F).

3.2. Evaluation of piezoelectric, photothermal and acoustodynamic properties

The piezoelectric properties of BNT and BNT@MoS₂ were measured using PFM (Fig. 2A and B). The phase hysteresis loop of PFM exhibited a 180° change under DC voltage, indicating the ferroelectric polarization conversion process. The butterfly curve voltage variation of BNT@MoS₂ was comparatively smaller and exhibited a higher amplitude when compared to BNT, indicating its superior piezoelectric property.

The photothermal properties were explored by monitoring the real-time temperature of different samples in PBS under 1060 nm laser irradiation. The increase of temperature is related to the extension of irradiation time (Fig. 3A). After 10 min of laser irradiation, the temperature of BNT only rose to 25 °C, while the temperature of BNT@MoS₂ reached 53.1 °C, indicating that BNT@MoS₂ had great photothermal conversion performance, which was mainly due to the excellent absorption of NIR by MoS₂. The photothermal effect of BNT@MoS₂ was influenced by laser power and sample concentration. Increasing the power density of the 1060 nm laser from 0.6 W/cm² to 1.0 W/cm² resulted in a rapid temperature rise at BNT@MoS₂, with values increasing from 42.8 °C to 63.1 °C (Fig. 3B). Similarly, elevating the sample concentration from 0.5 mg/mL to 1.5 mg/mL led to an increase in temperature at BNT@MoS₂, ranging from 41 °C to 65 °C (Fig. 3C).

The sonodynamic effect was evaluated by ESR to detect the generation of two ROS (¹O₂ and ·OH) under US irradiation. As shown in Fig. 3D and E, BNT can produce ROS under ultrasonic action, but after combining with MoS₂, the characteristic peak intensity increases significantly, and the ROS production increases significantly. The combination of MoS₂ and BNT served as an effective transmission platform for charge transfer, resulting in improved acoustodynamic performance (Fig. 3F). Under ultrasonic action, electrons were generated in the valence band of MoS₂ and subsequently transferred to the conduction band, creating holes in the conduction band. BNT acted as an electronic receiver, and due to the high conduction band of MoS₂, electrons were quickly transferred to the conduction band of BNT. The electrons then reacted with O₂ to produce ¹O₂, while the holes oxidized water to ·OH [10].

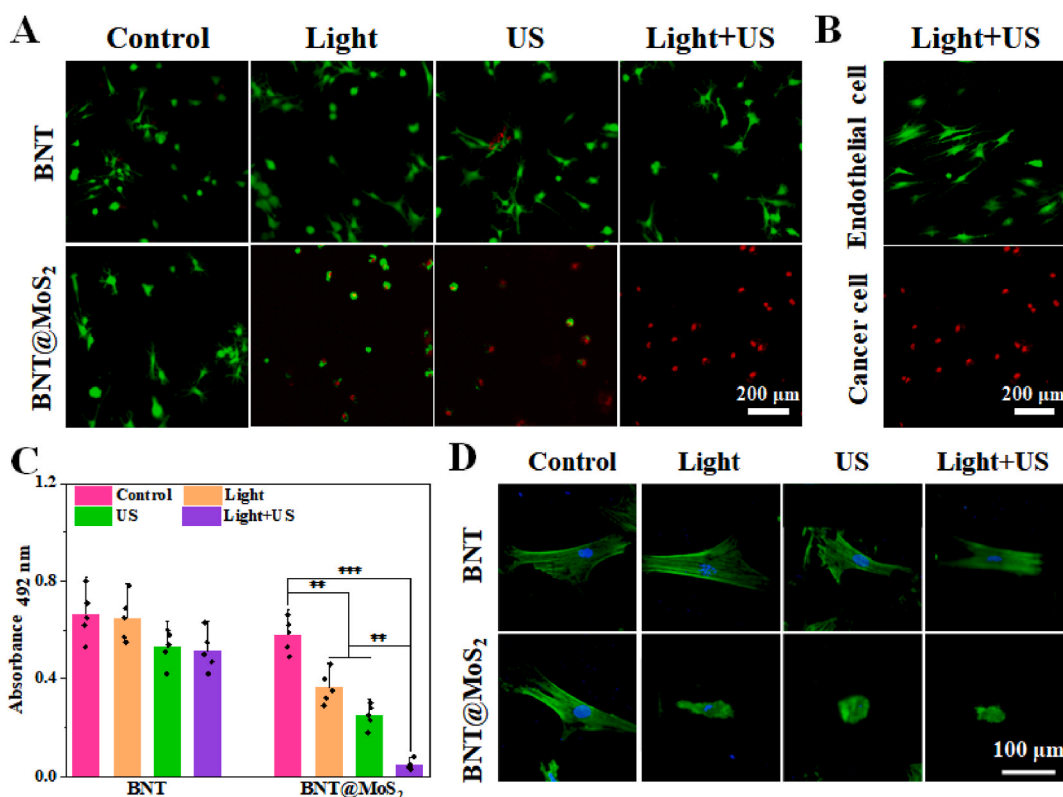


Fig. 4. Breast cells ablation of BNT and BNT@MoS₂: (A) Fluorescence images of breast cells and (B) endothelial cells; (C) MTT assay and (D) cytoskeleton staining of breast cells (* $p < 0.05$, *** $p < 0.001$).

3.3. The therapeutic effect of BNT@MoS₂ on breast cancer

Live/dead staining was performed to analyze the killing ability of BNT@MoS₂ on breast cells irradiated at 1060 nm laser and US. Fig. 4A demonstrated that in the BNT group, a limited number of deceased cells were observed solely under US irradiation or light + US irradiation. This suggested that a small quantity of ROS was insufficient to induce a widespread and rapid demise of cancer cells within a brief period. Conversely, in the BNT@MoS₂ group, all cells exhibited green fluorescence only in the absence of treatment. Under light or US irradiation, some cells were found to be deceased, while all cancer cells perished under light + US irradiation. This indicated that both PTT and SDT could inflict damage upon cancer cells, and their combined effect can efficiently eliminate cancer cells within a short timeframe. Fortunately, PTT and SDT cannot kill normal cells when they combine to kill cancer cells (Fig. 4B). The main reason may be that tumor cells were more sensitive to heat than normal cells [15,16]. The results of MTT were in substantial agreement with live/dead fluorescence staining, demonstrating pronounced toxicity to breast cells of BNT@MoS₂ solely under the combined irradiation of a 1060 nm laser + US (Fig. 4C). The morphology of cells after different treatments further verified the result (Fig. 4D). After being treated with Light, US and Light + US respectively, the diffusion area of cells in BNT@MoS₂ group was significantly reduced, especially the cells in Light + US group were reduced to a small ball.

4. Conclusion

In summary, the BNT@MoS₂ composites designed have excellent photothermal and acoustic properties. Under the irradiation of NIR-II laser and US, the combined action of PTT and SDT can eliminate breast cancer cells in 10 min. This study provides a potential therapeutic strategy for breast cancer.

Data availability

Data will be made available on request.

CRediT authorship contribution statement

Rong Li: Writing – original draft, Methodology, Data curation, Conceptualization. **Hao Liu:** Investigation, Data curation. **Xiudong**

Guo: Supervision, Investigation. **Xin yang:** Visualization. **Hailiang Zhang:** Supervision, Data curation. **Jianbo Song:** Writing – review & editing, Visualization, Data curation. **Guannan Zhang:** Writing – review & editing, Supervision, Funding acquisition.

Declaration of competing interest

The authors declare that they have no known competing financial interests or personal relationships that could have appeared to influence the work reported in this paper.

Guannan Zhang reports financial support was provided by Science and Technology Department of Shaanxi Province. If there are other authors, they declare that they have no known competing financial interests or personal relationships that could have appeared to influence the work reported in this paper.

Acknowledgments

This work was supported by Basic Projects in Research of Shanxi (Projects of Free Exploration, 202203021212095), Talent Activation Fund of Shanxi Bethune Hospital (2022RC03), Central Leading Science and Technology Development Foundation of Shanxi Province (YDZJSX20231A064).

References

- [1] K.D. Miller, L. Nogueira, T. Devasia, A.B. Mariotto, K.R. Yabroff, A. Jemal, J. Kramer, R.L. Siegel, Cancer treatment and survivorship statistics, *CA Cancer J. Clin* 72 (2022) 409–436.
- [2] X. Han, J. Huang, X. Jing, D. Yang, H. Lin, Z. Lin, P. Li, Y. Chen, Oxygen-deficient black titania for synergistic/enhanced sonodynamic and photoinduced cancer therapy at near infrared-II biowindow, *ACS Nano* 12 (2018) 4545–4555.
- [3] C. Dai, S. Zhang, Z. Liu, R. Wu, Y. Wu, Two-dimensional graphene augments nanosensitized sonocatalytic tumor eradication, *ACS Nano* 11 (2017) 9467–9480.
- [4] G.N. Zhang, Y.Q. Yang, J. Shi, X.H. Yao, W.Y. Chen, X.C. Wei, X.Y. Zhang, P.K. Chu, Near-infrared light II-assisted rapid biofilm elimination platform for bone implants at mild temperature, *Biomaterials* 269 (2021) 120634.
- [5] P. Zhu, Y. Chen, J. Shi, Piezocatalytic tumor therapy by ultrasound-triggered and BaTiO₃-mediated piezoelectricity, *Adv. Mater* 32 (2020) 2001976.
- [6] L. Shi, S. Sun, Y. Chen, P. Wang, J. Wang, X. Zhang, J. Zou, Z.L. Wang, Advances in piezo-phototronic effect enhanced photocatalysis and photoelectrocatalysis, *Adv. Energy Mater.* 10 (2020) 2000214.
- [7] B. Yang, Y. Chen, J. Shi, Reactive oxygen species (ROS)-based nanomedicine, *Chem. Rev* 119 (2019) 4881–4985.
- [8] J. Sun, C. Shen, J. Guo, H. Guo, Y. Yin, X. Xu, Z. Fei, Z. Liu, X. Wen, Highly efficient activation of peroxymonosulfate by Co₃O₄/Bi₂WO₆ pn heterojunction composites for the degradation of ciprofloxacin under visible light irradiation, *J. Colloid Interface Sci.* 588 (2021) 19–30.
- [9] A. Ranjan, K.Y. Hsiao, C.Y. Lin, Y.H. Tseng, M.Y. Lu, Enhanced piezocatalytic activity in Bi_{1/2}Na_{1/2}TiO₃ for water splitting by oxygen vacancy engineering, *ACS Appl. Mater. Interfaces* 14 (2022) 35635–35644.
- [10] G.N. Zhang, X.Y. Zhang, Y.Q. Yang, R.F. Chi, J. Shi, R.Q. Hang, X.B. Huang, X.H. Yao, P.K. Chu, X.Y. Zhang, Dual lights-induced in situ antibacterial activities of biocompatible TiO₂/MoS₂/PDA/RGD nanorod arrays on titanium, *Biomater. Sci.* 8 (2020) 391–404.
- [11] Z. Zhou, B.W. Li, C. Shen, D. Wu, H.C. Fan, J.Q. Zhao, H. Li, Z.Y. Zeng, Z.M. Luo, L.F. Ma, C.L. Tan, Metallic 1T phase enabling MoS₂ nanodots as an efficient agent for photoacoustic imaging guided photothermal therapy in the near-infrared-II window, *Small* 16 (2020), 2004173.
- [12] H.Z. Chen, X.J. He, Z. Zhou, Z.K. Wu, H. Li, X.S. Peng, Y.B. Zhou, C.L. Tan, J.L. Shen, Metallic phase enabling MoS₂ nanosheets as an efficient sonosensitizer for photothermal-enhanced sonodynamic antibacterial therapy, *J. Nanobiotechnol.* 20 (2022) 136.
- [13] C. Wang, J. Lei, C. Mao, S. Wu, Y. Zheng, C. Liang, L. Yang, S. Zhu, Z. Li, H. Jiang, Y. Zhang, C. Yang, X. Liu, Defective S-TiO_{2-x}/CeO₂ heterojunction for mutual reinforcing chemodynamic/sonocatalytic antibacterial therapy and sonoelectric/ion-activated bone regeneration, *Adv. Funct. Mater.* 33 (2023) 2306493.
- [14] Y.C. Zhao, S.B. Wang, Y.M. Ding, Z.Y. Zhang, T. Huang, Y.L. Zhang, X.Y. Wan, Z.L. Wang, L.L. Li, Piezotronic effect-Augmented Cu₂-XO-BaTiO₃ sonosensitizers for multifunctional cancer dynamic therapy, *ACS Nano* 16 (2022) 9304–9316.
- [15] G.N. Zhang, Z.Z. Wu, Y.Q. Wu, J. Shi, J. Lv, Y. Fang, Z. Shen, Z. Shen, P.C. Li, X.H. Yao, W.Y. Chen, X.C. Wei, P.K. Chu, X.Y. Zhang, A multifunctional antibacterial coating on bone implants for osteosarcoma therapy and enhanced osteointegration, *Chem. Eng. J* 428 (2022) 131155.
- [16] G.N. Zhang, Y. Lu, J.B. Song, D. Huang, M.W. An, W.Y. Chen, P.D. Han, X.H. Yao, X.Y. Zhang, A multifunctional nano-hydroxyapatite/MXene scaffold for the photothermal/dynamic treatment of bone tumours and simultaneous tissue regeneration, *J. Colloid Interface Sci.* 652 (2023) 1673–1684.